THE JOURNAL OF PHYSICAL CHEMISTRY C

ARTICLE

pubs.acs.org/JPCC

Designing a Red Persistent Luminescence Phosphor: The Example of $YPO_4:Pr^{3+},Ln^{3+}$ (Ln = Nd, Er, Ho, Dy)

A. Lecointre,[†] A. Bessière,[*,†,§] A. J. J. Bos,[‡] P. Dorenbos,[‡] B. Viana,[†] and S. Jacquart[†,§]

[†]Ecole Nationale Supérieure de Chimie de Paris (Chimie ParisTech), Laboratoire de Chimie de la Matière Condensée de Paris (UMR 7574 CNRS), 11 Rue P&M Curie, 75231 Paris Cedex 05, France

[‡]Luminescence Materials Research group, Faculty of Applied Sciences, Delft University of Technology, Mekelweg 15, 2629 JB Delft, The Netherlands

[§]Department of Physics, Goa University, Taleigao Plateau, Goa 403 206, India

ABSTRACT: Yttrium phosphates codoped (Ce^{3+},Ln^{3+}) and (Pr^{3+},Ln^{3+}) with Ln = Nd, Er, Ho, Dy were investigated by thermally stimulated luminescence. Similar to Ce^{3+}, Pr^{3+} was found able to trap holes up to high temperatures while being the radiative recombination center, whereas the Ln^{3+} codopant played the role of the electron trap. Trapping depths for all studied Ln^{3+} (Ln = Ce, Pr, Nd, Er, Ho, Dy) were found to follow the Ln^{2+} energy levels prediction. Low-temperature electron trapping at Ce^{3+} and Pr^{3+} was, therefore, evidenced for the first time at 0.20−0.27 and 0.58 eV, respectively. The 195 K peak was attributed to self-trapped charges in YPO_4, whereas the 480 K peak was uniquely associated with praseodymium doping. Pr^{3+} as the luminescent center and Nd^{3+}/Er^{3+}/Ho^{3+}/Dy^{3+} as the codopant were selected to design a red persistent luminescence phosphor. The best persistent luminescence was obtained as predicted by the model for Ho^{3+} codoping, though it was shown to originate from both thermally assisted detrapping from (Pr^{3+},Ho^{3+}) and athermal tunneling recombination.

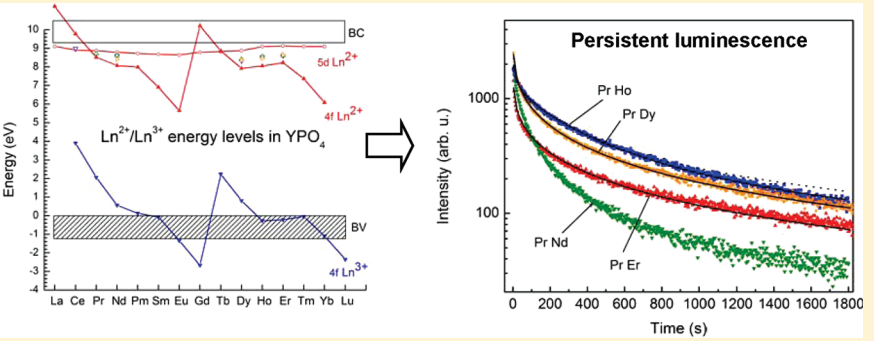

I. INTRODUCTION

Since the discovery by Matsuzawa et al. of a new persistent phosphor $SrAl_2O_4:Eu^{2+},Dy^{3+}$[1] able to emit bright light for hours after the end of the excitation in the mid-1990s, the research for new phosphorescent compounds has become increasingly popular. However, among the known persistent luminescence compounds, only a few, such as $CaS:Eu^{2+},Tm^{3+}$ emitting at 650 nm,[2] $CaTiO_3:Pr^{3+}$ at 615 nm,[3] $MgSiO_3:Eu^{2+},Mn^{2+},Dy^{3+}$ at 660 nm,[4] $ZnS:Mn^{2+}$ at 600 nm,[5] $Y_2O_2S:Eu^{3+},Mg^{2+},Ti^{4+}$ at 627 nm,[6] $Ca_2Si_5N_8:Eu^{2+}$ at 620 nm,[7] and $Ca_2SiO_4:Eu^{2+},Nd^{3+}$ at 660 nm,[8] emit in the orange to near-infrared spectral range. Though green emitters are indeed very much needed in applications, such as emergency signing, as they match the maximum of sensitivity of human vision, much interest would arise from red persistent phosphors. There is still a general lack of understanding of persistent luminescence mechanisms, and diversifying the emitting ions may be useful to the general comprehension of the phenomenon. Besides the lack of red persistent phosphors for visual signing, a novel application for red-infrared persistent luminescence was recently developed in the exciting field of in vivo imaging.[9,10] Red-emitting long-lasting phosphorescent nanoparticles were used as biomarkers injected in the vascular system of a mouse. Exciting these biomarkers outside the animal body prior to their injection prevents any phenomenon of tissue autofluorescence, which is a tremendous advantage over classical fluorescent markers. A very important requirement for the long-lasting phosphorescent biomarker is to emit light between 600 and 1100 nm as the animal tissues are transparent in this optical range. For these reasons, in the past recent years, we have been focusing our interest on new persistent luminescence phosphors emitting in the orange-to-near-infrared region.[11−13]

Because of their high thermal and chemical stabilities,[14] the compounds APO_4 (A = Y, La, Gd, Lu) have been largely investigated.[15−17] Rare earth-activated APO_4 have attracted great interest because of their marked improvement in lumen output and color-rendering index in fluorescence lamps and display devices.[18−21] More recently, a comprehensive thermally stimulated luminescence (TSL) study revealed that (Ce^{3+}, Ln^{3+}) codoped yttrium phosphates can act as charge storage phosphors.[22] Charge carrier trapping by trivalent lanthanide ions is determined by the location of the ground state of the divalent and trivalent lanthanides relative to the valence and conduction bands of the host material. Dorenbos has developed a semiempirical model that describes the systematic energy positions of

Received: August 25, 2010
Revised: January 10, 2011
Published: February 21, 2011

Ln^{2+} and Ln^{3+} ground states relative to the valence and conduction bands[23−25] and has provided insight into how specific pairs of Ln^{3+} ions in YPO_4 can work together to efficiently store and release charges.[22,26] By measuring trap depths in $YPO_4:Ce^{3+},Ln^{3+}$ with the help of TSL experiments[22,27] or synchrotron−laser excitation spectroscopy,[28] the accuracy of the model developed by Dorenbos has been checked. The model predicts, for instance, that Ce^{3+} is a stable hole trap, whereas certain other trivalent lanthanides, such as Nd^{3+}, Dy^{3+}, Ho^{3+}, Er^{3+}, Tm^{3+}, and Sm^{3+}, act as more shallow electron traps. Ce^{3+} ions together with other Ln^{3+} codoping ions, therefore, act as efficient charge trapping couples. After high-energy excitation, a multitude of electrons are raised from the valence band to the conduction band. When the ground state of a divalent lanthanide is located below the bottom of the conduction band, the corresponding trivalent lanthanide is able to trap an electron according to the scheme: $Ln^{3+} + e \rightarrow Ln^{2+}$. The holes, in contrast, are trapped at Ce^{3+} doping ions, according to the scheme: $Ce^{3+} + h \rightarrow Ce^{4+}$. By thermal activation, the trapped electrons are transferred back to cerium where they recombine radiatively with the hole left behind and generate Ce^{3+} 5d−4f luminescence according to the scheme: $Ce^{4+} + e \rightarrow (Ce^{3+})^* \rightarrow Ce^{3+} + h\nu$.

In practice, persistent luminescence observed at room temperature is most often associated with TSL occurring between 300 and 420 K. This most usually corresponds to charge trapping at energy depths between 0.6 and 2.0 eV. In $YPO_4:Ce^{3+},Ln^{3+}$, electrons are trapped at Ln^{3+} according to the scheme $Ln^{3+} + e \rightarrow Ln^{2+}$. Dorenbos and Bos demonstrated that the trap depth of Ln^{3+} as an electron trap was very close to the energy difference between the ground state of Ln^{2+} and the bottom of the conduction band.[29] Dorenbos's model showed that the fundamental energy levels of Nd^{2+}, Dy^{2+}, Ho^{2+}, and Er^{2+} were located at around 1 eV below the bottom of the conduction band.[28] Hence, the corresponding Ln^{3+} ions (Ln = Nd, Dy, Ho, Er) were selected here as potential codopants to obtain persistent luminescence at room temperature.

The characteristic 5d−4f emission of Ce^{3+} in YPO_4 is located in the ultraviolet region. To obtain red luminescence, another recombination center (and hole trap) than Ce^{3+} must be considered. By looking at the predicted energy level scheme,[28] Tb^{3+} and Pr^{3+} are two other possible candidates to be stable hole traps in YPO_4 at room temperature because their ground state is located at 2.24 and 2.06 eV, respectively, above the top of the valence band. Tb^{3+} mainly emits in the green region via the $^5D_4 \rightarrow {}^7F_5$ transition,[30] whereas Pr^{3+} presents several emissions from the 4f excited $^3P_0$ state mainly in the blue and from the $^1D_2$ level in the red.[31,32] Multiphonon processes occurring from $^3P_0$ to $^1D_2$ have been shown to promote the red emission in the YPO_4 lattice.[31−34] We, therefore, decided to use Pr^{3+} as the radiative recombination center to try and obtain red persistent luminescence in YPO_4.

This paper presents the TSL properties over a wide temperature range of Ce^{3+},Ln^{3+}-codoped and Pr^{3+},Ln^{3+}-codoped YPO_4 (Ln = Nd, Er, Ho, and Dy). It unravels complementary data to the previous TSL studies, in particular, by identifying new low-temperature peaks related to the host or to a special dopant and by evidencing tunneling effects that should be taken into consideration in the design of persistent phosphors. The persistent luminescence of the red-emitting Pr^{3+},Ln^{3+}-codoped YPO_4 compounds was measured and is analyzed in relation with the TSL results. The nature of the traps in $YPO_4:Ce^{3+},Ln^{3+}$ and $YPO_4:Pr^{3+},Ln^{3+}$ is discussed, and some mechanisms of delayed luminescence of $YPO_4:Pr^{3+},Ln^{3+}$ are elucidated. The potential of $YPO_4:Pr^{3+},Ln^{3+}$ as a red persistent phosphor is discussed.

II. EXPERIMENTAL METHODS

A. Sample Preparation. Powder samples of yttrium phosphate were synthesized by a solid-state reaction. The raw materials were yttrium oxide (Y_2O_3), ammonium dihydrogenophosphate ($NH_4H_2PO_4$), cerium fluoride (CeF_3), and lanthanide oxides (Ln_2O_3 for Ln = Ho, Nd, Er, Dy, and Pr_6O_{11}). The nominal lanthanide concentrations were 0.5 at. % relative to yttrium. The powders were mixed and heated up at 400 °C for 10 h to eliminate the volatile H_2O and NH_3. The powders were then carefully mixed again and calcinated at 1400 °C for 5 h in order to complete the reaction. The samples' purity was checked by X-ray diffraction with an X'PERT PRO X-ray diffractometer working with Cu Kα radiation. YPO_4 has the tetragonal zircon structure with a single cationic site for Y^{3+}. The metal atom Y^{3+} is coordinated by eight oxygen atoms, forming a polyhedron with a site symmetry D_{2d}.[33]

B. Measurement Techniques. Excitation and emission spectra were recorded with a Varian Cary Eclipse Fluorescence spectrophotometer at room temperature. Long-lasting luminescence and thermally stimulated luminescence (TSL) measurements were carried out on 13 mm diameter pellets presenting a thickness of 1 mm made of the powder samples. Light was collected via an optical fiber by a Roper Scientific Pixis 100 CCD camera cooled at −68 °C coupled with an Acton SpectraPro 2150i spectrometer for spectral analysis. Long-lasting luminescence spectra were recorded every 3 s after 10 min of irradiation with an X-ray molybdene tube operating at 50 kV and 20 mA. In TSL, the pellet is silver glued on the cold finger of a closed cycle helium cryogenerator. X-ray irradiation is performed at 30 K through a thin beryllium window of the cryogenerator at a 45° angle from the pellet surface, and luminescence is detected through a quartz window of the cryostat at a 45° angle from the pellet surface. A heating rate of 10 K/min was applied. A homemade software enables us to present TSL results as three-dimensional plots (wavelength, temperature, intensity).

III. RESULTS

A. Photoluminescence. Excitation and emission spectra of $YPO_4:Ce^{3+}$ recorded at room temperature are shown in Figure 1a. The excitation spectrum for emission fixed at 357 nm shows four bands with maxima at 323, 250, 238, and 224 nm and possibly another one around 200 nm. These five absorption bands correspond to the 4f−5d transitions of Ce^{3+} whose 5d orbitals are split by the crystal field created by oxygen neighbors at the Y^{3+} site of symmetry D_{2d}.[34] The emission spectrum after excitation at 252 nm shows two bands at 333 and 356 nm showing a Stokes shift of about 930 cm^{-1}. The emission is due to transitions from the lowest 5d level to the $^2F_{5/2}$ and $^2F_{7/2}$ spin−orbit split states of Ce^{3+}.[35,36]

Excitation and emission spectra of $YPO_4:Pr^{3+}$ recorded at room temperature are shown in Figure 1b. The excitation spectrum for emission set at 597 nm shows three peaks at 450, 475, and 486 nm corresponding to, respectively, $^3H_4 \rightarrow {}^3P_2$, $^3H_4 \rightarrow {}^3P_1$, and $^3H_4 \rightarrow {}^3P_0$ 4f−4f transitions of Pr^{3+}. After excitation at 450 nm into the $^3P_2$ level of Pr^{3+}, several f−f transitions are observed on the emission spectrum. Luminescence in the orange

and red regions of the spectrum is actually observed through the $^1D_2 \rightarrow {}^3H_4$, $^3P_0 \rightarrow {}^3H_6$, and $^3P_0 \rightarrow {}^3F_2$ transitions of Pr^{3+}.

B. Thermally Stimulated Luminescence. *i. Ce^{3+}, Ln^{3+}-Co-doped YPO_4.* In Figure 2, the TSL glow curves of YPO_4:Ce^{3+}, Er^{3+} and YPO_4:Ce^{3+},Dy^{3+} are plotted wavelength-resolved in a two-dimensional $\lambda - T$ plot. For all (Ce^{3+},Ln^{3+})-codoped YPO_4,

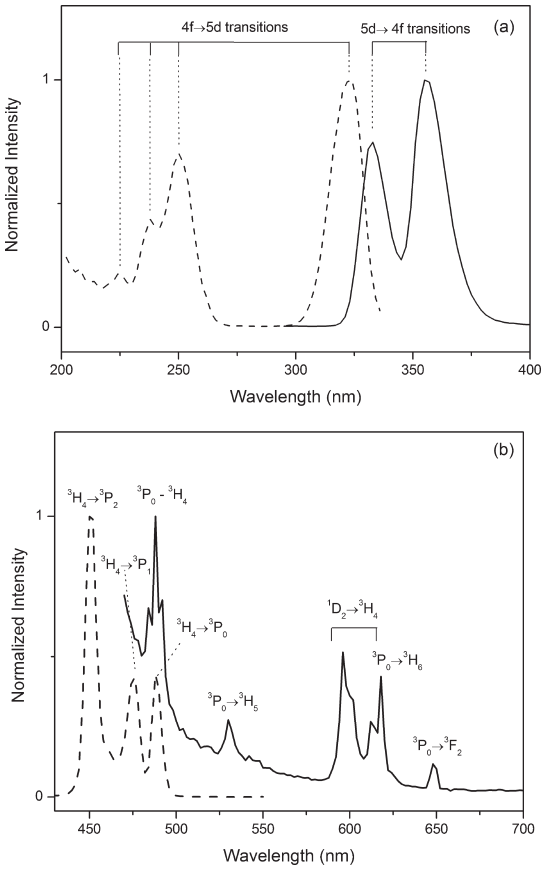

Figure 1. (a) Excitation spectrum (dotted line) for emission monitored at 357 nm and emission spectrum (solid line) excited at 252 nm of YPO_4:Ce^{3+}. (b) Excitation spectrum (dotted line) for emission monitored at 597 nm and emission spectrum (solid line) excited at 450 nm of YPO_4:Pr^{3+} recorded at room temperature.

the characteristic 5d−4f emission doublet of Ce^{3+} is observed at 333 and 357 nm, as indicated in Figure 2a, with weak second-order bands around 670 and 715 nm due to the diffraction grating of the monochromator. In addition to the 5d−4f emission of Ce^{3+}, YPO_4:Ce^{3+},Dy^{3+} presents intense emission lines at 481 and 575 nm (see Figure 2b). These lines are characteristic for the $^4F_{9/2} \rightarrow (^6H_{15/2}, {}^6H_{13/2})$ transitions of Dy^{3+}.[18,37]

The normalized TSL glow curves of Ce^{3+} emission (monitored at 333 nm) for YPO_4:Ce^{3+} and YPO_4:Ce^{3+},Ln^{3+} (Ln = Er, Nd, Ho, and Dy) are shown in Figure 3. They present three peaks located, respectively, at around 100 K for peak A, at around 120 K for lower intensity peak A′, and at around 195 K for peak B for all the compounds. The Ln^{3+}-codoped compounds present a third peak denoted as X'_{LN}, in which the temperature of the maximum varies between 250 and 400 K according to the Ln^{3+} codopant. The temperature for maximum intensity T_m of this peak increases in the order of the codopant $Er^{3+} < Nd^{3+} < Ho^{3+} < Dy^{3+}$. Such a variation of T_m accordingly with the codopant was first reported by Bos et al. in a TSL experiment run on YPO_4:Ce^{3+},Ln^{3+} powders from room temperature and with a faster heating rate (5 °C/s). They observed a peak position varying in the order $Er^{3+} < Nd^{3+} < Ho^{3+} < Dy^{3+} < Sm^{3+} < Tm^{3+} < Yb^{3+}$.[22] A small extra peak denoted as C is present on YPO_4:Ce^{3+},Nd^{3+} at 135 K.

In Figure 3, a background of TSL intensity is also clearly visible below room temperature. A TSL intensity of around 10−20% of the maximum intensity of the X_{Ln} peak is present at 50 K for all the compounds. Such a background is actually partly due to the tail of a luminescence decay that can be clearly distinguished between 30 and 70 K. Such a decay at the beginning of a TSL curve has already been observed on other Ce-doped materials, such as $YAlO_3$:Ce,[38] for instance, and attributed to radiative recombination by athermal tunneling.[39] Note that the same trapping couple can give rise to both tunneling recombination and classical thermally assisted detrapping.[27,40] If the same traps are involved in tunneling as well as in thermally assisted detrapping characterized by a TSL peak, no tunneling recombination will be observed at temperatures higher than the TSL peak because all charges will have been detrapped during the thermally assisted process. For the monodoped compound YPO_4:Ce^{3+}, the TSL background disappears after peaks A/A′. Tunneling

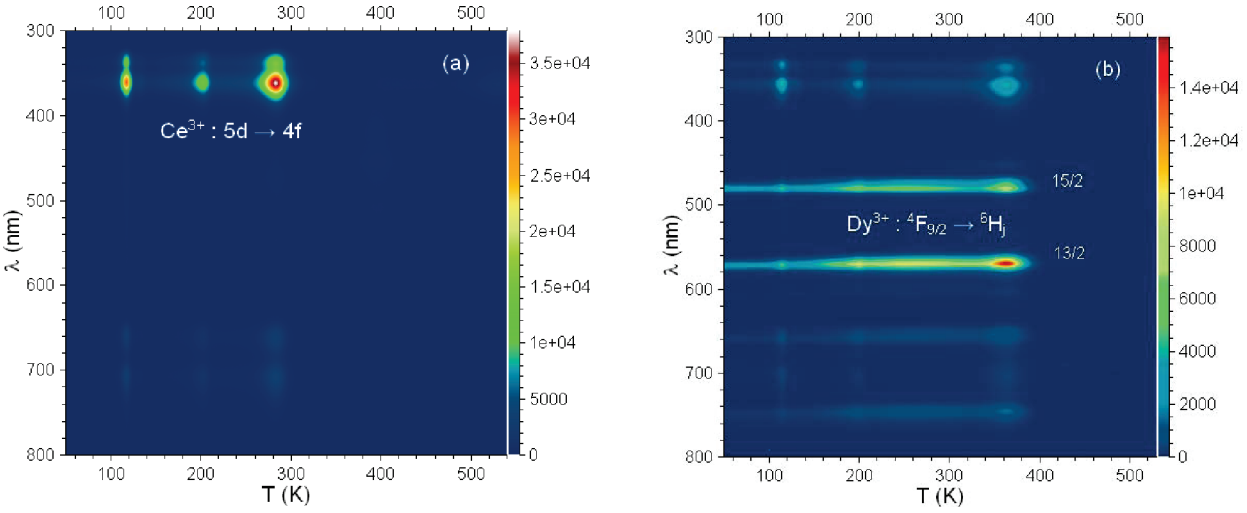

Figure 2. Wavelength (λ)/temperature (T) contour plots of (a) YPO_4:Ce^{3+},Er^{3+} and (b) YPO_4:Ce^{3+},Dy^{3+} after 10 min of X-ray irradiation.

dx.doi.org/10.1021/jp108038v |J. Phys. Chem. C 2011, 115, 4217–4227

recombination, therefore, concerns charges involved in the recombination of peaks A/A′. For all others, it disappears after peak X'_{LN}, and tunneling, therefore, occurs between charges detrapped at X_{Ln}. The nature of the traps will be discussed further in the paper.

Note that this TSL background in Figure 3 is actually not constant or slightly decreasing with time/temperature between 30 K and room temperature as would be expected from a mere athermal tunneling mechanism. For all samples, after a decaying intensity up to 50−70 K, the TSL intensity increases as the temperature goes up to the related TSL peak (A/A′ in the case of $YPO_4:Ce^{3+}$ and X_{Ln} in the case of $YPO_4:Ce^{3+},Ln^{3+}$). This is particularly the case for $YPO_4:Ce^{3+},Nd^{3+}$. Hence, some thermally assisted processes appear to be at stake in addition to the athermal tunneling emission. An explanation for that will be proposed in the Discussion section.

ii. Pr^{3+},Ln^{3+}-Codoped YPO_4. In Figure 4, the TSL glow curves of $YPO_4:Pr^{3+},Ho^{3+}$ and $YPO_4:Pr^{3+},Dy^{3+}$ are plotted wavelength-resolved in a two-dimensional $\lambda-T$ plot. The $YPO_4:Pr^{3+}$ and $YPO_4:Pr^{3+},Ln^{3+}$ (Ln = Ho, Er, Nd, Dy) curves mainly display 4f−4f emission lines of Pr^{3+} at 488, 598−612, 618, and 649 nm corresponding to the $^3P_0 \rightarrow {}^3H_4$, $^1D_2 \rightarrow {}^3H_4$, $^3P_0 \rightarrow {}^3H_6$, and $^3P_0 \rightarrow {}^3F_2$ transitions, respectively. An additional broader emission band is observed at 450 nm. The band was observed in radioluminescence with a high intensity at low temperature and a reduced intensity at room temperature. This is attributed to a host-related emission band. A similar band was also observed on radioluminescence spectra of Ce^{3+}-doped YPO_4 at low temperature. However, in Ce^{3+}-doped YPO_4, this band is totally suppressed at room temperature and not observed in TSL spectra.

The TSL curves for Pr^{3+} emission monitored at 612 nm are shown in Figure 5. All the curves present two peaks, respectively, at around 195 K (denoted as peak B′) and at around 480 K (denoted as peak D). Additionally to these two features, a third peak X'_{Ln} is observed in which the temperature of the maximum varies between 250 and 400 K according to the lanthanide ion. The temperature for maximum intensity increases in the exact same order as that for the Ce^{3+}, Ln^{3+}-doped compounds, that is, $Er^{3+} < Nd^{3+} < Ho^{3+} < Dy^{3+}$. For the monodoped sample, an extra peak at 252 K (peak E) is observed. Similar to $YPO_4:Ce^{3+}$, Nd^{3+}, an extra peak at 135 K denoted as peak C′ is observed only in $YPO_4:Pr^{3+},Nd^{3+}$.

As for the Ce-doped samples, tunneling recombination is observed in Pr-doped compounds through a quite intense TSL

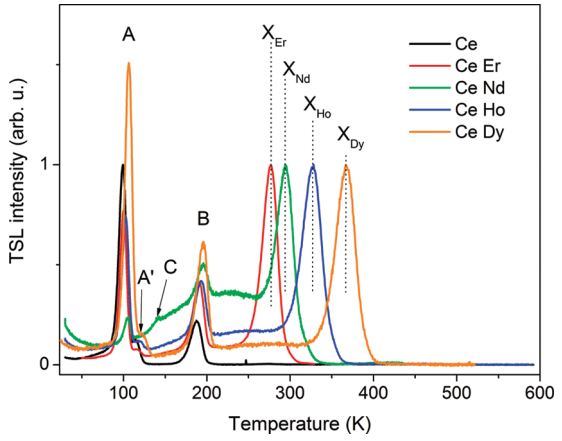

Figure 3. Normalized TSL glow curves of $YPO_4:Ce^{3+}$ and $YPO_4:Ce^{3+}$, Ln^{3+} (Ln = Er, Nd, Ho, Dy) monitoring Ce^{3+} emission at 333 nm.

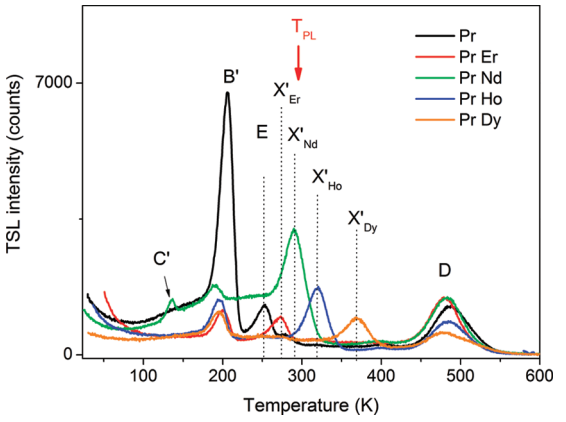

Figure 5. TSL glow curves of $YPO_4:Pr^{3+}$ and $YPO_4:Pr^{3+},Ln^{3+}$ (Ln = Er, Nd, Ho, Dy) monitoring Pr^{3+} emission at 612 nm.

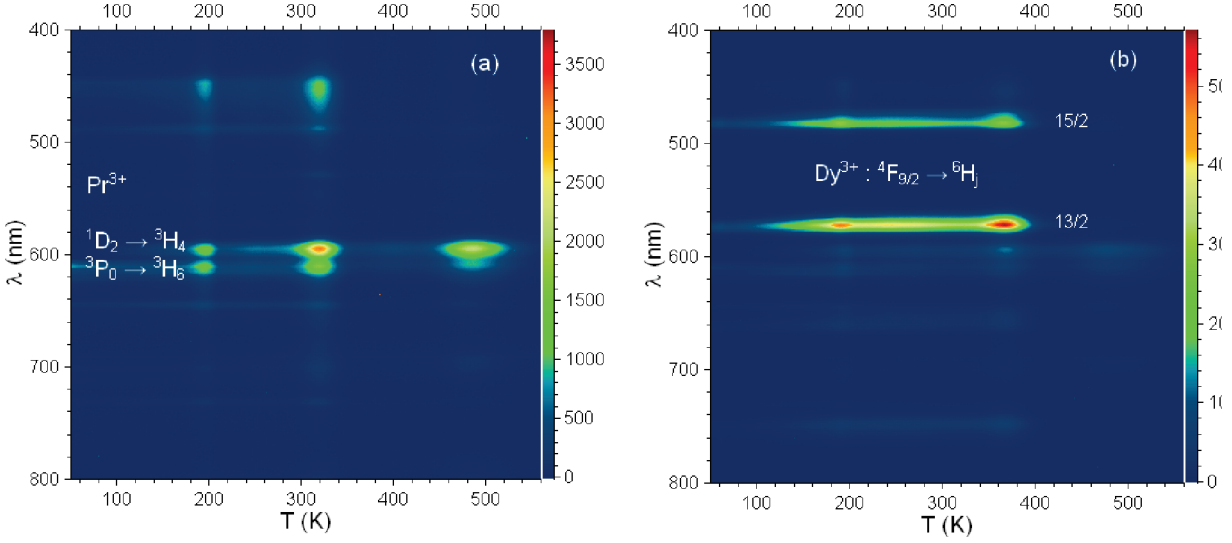

Figure 4. Wavelength (λ)/temperature (T) contour plots of (a) $YPO_4:Pr^{3+},Ho^{3+}$ and (b) $YPO_4:Pr^{3+},Dy^{3+}$ after 10 min of X-ray irradiation.

dx.doi.org/10.1021/jp108038v |J. Phys. Chem. C 2011, 115, 4217–4227

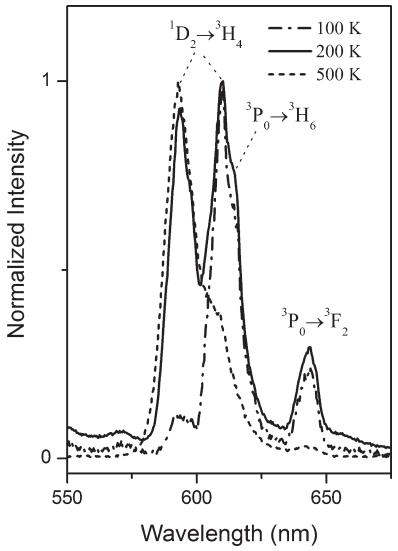

Figure 6. Normalized TSL spectra of $YPO_4:Pr^{3+}$ at different temperatures during the TSL measurement.

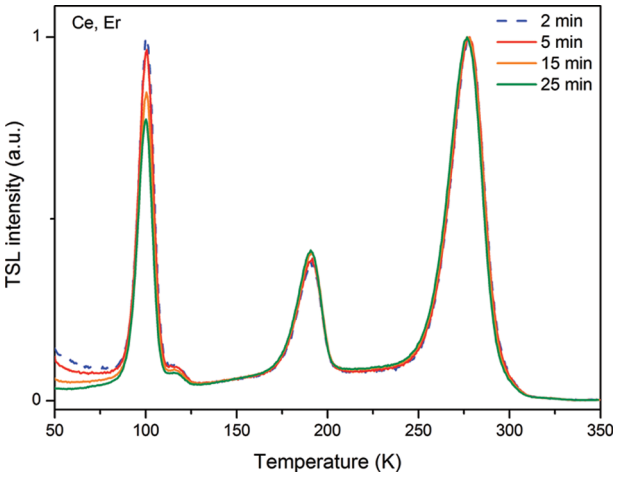

Figure 7. TSL glow curves of $YPO_4:Ce^{3+},Er^{3+}$ recording Ce^{3+} emission at 333 nm after different irradiation times.

background. The decay of the athermal tunneling recombination is very well observed below 100 K for all samples. Note that a variable delay of around 3 min between the end of the irradiation and the start of the heating ramp was unintentionally applied, explaining the different decaying behaviors below 100 K. Although the TSL background was found to be suppressed after peaks A/A′ and X_{Ln} in Ce-doped YPO_4, it is not true in Pr-doped YPO_4 after peak X'_{Ln}. The background is partially reduced after X'_{Ln}, more or less depending on the codopants. It is only after peak D that tunneling emission is totally suppressed for all samples. Hence, a large part of tunneling occurs through the trapping system at stake in peak D.

As for the Ce-doped sample, some thermally activated processes superimpose over the athermal tunneling background. Again, this is particularly clear for $YPO_4:Pr^{3+},Nd^{3+}$, which presents an increasing background intensity between 100 and 300 K.

Note that the emission spectrum of Pr^{3+}-doped compounds changes along with temperature during the TSL experiment. At low temperature, the samples emit white light, which results from a mixture of the following Pr^{3+} emission lines: the $^3P_0 \rightarrow {}^3H_4$ transition in the blue region, the $^3P_0 \rightarrow {}^3H_5$ transition in the green region, and the $^1D_2 \rightarrow {}^3H_4$ and $^3P_0 \rightarrow {}^3H_6$ transitions in the orange-red region. At room temperature, they emit an orange-red light. A zoom of the 550−650 nm range for TSL spectra at 100, 200, and 500 K is shown in Figure 6. As the temperature increases, the emission from $^1D_2$ becomes more important relative to emissions from $^3P_0$. In yttrium phosphate, only four phonons are needed to match up the energy difference between $^3P_0$ and $^1D_2$ levels (about 4000 cm^{-1}).[15,33] With the multiphonon relaxation from $^3P_0$ to $^1D_2$, emissions from the $^3P_0$ level at 488, 530, 618, and 649 nm decrease, leaving alone the emission from the $^1D_2$ level and explaining the shift from a white light emission to an orange-red one. This is beneficial for the imaging application as red luminescence is looked for. Note, however, that, as seen in Figure 6, the multiphonon relaxation from $^3P_0$ to $^1D_2$ also shifts the maximum of emission from red toward orange.[31]

iii. Activation Energies. Assuming that the total number of trapped carriers is proportional to the radiation exposure time, $YPO_4:Ce^{3+},Er^{3+}$ as an instance was exposed to X-rays for various amounts of time at low temperature before a TSL experiment was run. The TSL glow curves obtained after various exposure times are shown in Figure 7. In Figure 7, the temperature of the maximum peak intensity T_m of all the three peaks observed was found constant when the exposure time was increased. T_m is, therefore, independent of the total number of initially trapped carriers, and the thermoluminescent phenomenon for each of these peaks can be considered as a first-order kinetic process. This means that retrapping is negligeable during heating, and a model of one trapping−one recombination center[41] can be applied for peaks A/A′, B, and X_{Ln}. As it was demonstrated for $YPO_4:Ce^{3+},Er^{3+}$, we assumed this to be also true for all other $YPO_4:Ce^{3+},Ln^{3+}$, which present the same nature of peaks (only the temperature position of X_{Ln} is shifting). We also assumed this for $YPO_4:Pr^{3+},Ln^{3+}$, as we demonstrate in the following section that peaks B and B′ on the one hand and peaks X_{Ln}, X'_{Ln}, and E on the other hand are of the same nature. Assumption over peak D is only tentative.

The activation energies of TSL peaks were determined by using the formula developed by Chen[42] based on the shape of the glow curve as this method provided satisfying results for the same compounds in ref 22. For first-order kinetics, the trap depth or activation energy E (in eV) can be calculated from

$$E = 2.52kT_m^2/\mathrm{fwhm} - 2kT_m^2 \qquad (1)$$

where k is the Boltzmann constant (eV/K), T_m the temperature (K) at the glow peak maximum, and fwhm the full width at half-maximum (K) of the glow peak. The calculated activation energies of peaks X_{Ln} for $YPO_4:Ce^{3+},Ln^{3+}$ and X'_{Ln} for $YPO_4:Pr^{3+},Ln^{3+}$ samples are reported in Table 1 together with the values found by Bos et al. for $YPO_4:Ce^{3+},Ln^{3+}$[22] and the most recent Ln^{2+} energy positions predicted by the Dorenbos energy level scheme.[28] In Table 2, activation energies of peaks still not identified (A, B, B′, E, and D) are reported. For peaks A′, C, and C′, we could not determine activation energies by the method based on the shape of the glow curve because they were displaying a too small intensity relative to the background activation energies. We, therefore, used a simpler approach. For the condition of the glow peak maximum of a first-order glow peak holds[43]

$$\beta E/kT_m^2 = s\exp(-E/kT_m) \quad \text{or}$$
$$E = s/\beta\{T_m \exp(-E/kT_m)\}kT_m \qquad (2)$$

where β (K/s) is the heating rate and s (s^{-1}) the frequency factor.

dx.doi.org/10.1021/jp108038v |J. Phys. Chem. C 2011, 115, 4217–4227

Table 1. Trap Depth and Uncertainty in eV of Ln^{3+} Codopants in $YPO_4:Ce^{3+},Ln^{3+}$ and in $YPO_4:Pr^{3+},Ln^{3+}$ Determined by the Peak Shape Method and Compared to the Literature

	trap depth (eV)			
codopant	$YPO_4:Ce^{3+},Ln^{3+}$ (this work)	$YPO_4:Pr^{3+},Ln^{3+}$ (this work)	$YPO_4:Ce^{3+},Ln^{3+}$ (Bos et al.[22])	energy level scheme prediction[28]
Er	0.70 ± 0.04	0.69 ± 0.06	0.65 ± 0.06	0.97
Nd	0.70 ± 0.08	0.68 ± 0.09	0.89 ± 0.09	1.12
Ho	0.76 ± 0.06	0.74 ± 0.06	0.84 ± 0.08	1.15
Dy	0.98 ± 0.04	0.89 ± 0.09	0.94 ± 0.07	1.28

Table 2. Trap Depth and Uncertainty in eV of Other TSL Peaks Observed in $YPO_4:Ce^{3+},Ln^{3+}$ and in $YPO_4:Pr^{3+},Ln^{3+}$. Proposed Attribution and Trapping Mechanism of the Peaks[a]

peak	T_m (K)	trap depth (eV)	luminescent center/trap *before trapping*	luminescent center/trap *after trapping*
A	100	0.20 ± 0.02	Ce^{3+}/Ce^{3+}	Ce^{4+}/Ce^{2+}
(A′)	(120)	(0.27 ± 0.04)		
C	135	0.31 ± 0.06	Ce^{3+}/Nd ?	Ce^{4+}/Nd ?
C′	135	0.31 ± 0.06	Pr^{3+}/Nd ?	Pr^{4+}/Nd ?
B	195	0.41 ± 0.08	Ce^{3+}/host	Ce^{4+}/self-trapped electron
B′	195	0.41 ± 0.08	Pr^{3+}/host	Pr^{4+}/self-trapped electron
E	252	0.58 ± 0.09	Pr^{3+}/Pr^{3+}	Pr^{4+}/Pr^{2+}
D	480	1.10 ± 0.06	Pr^{3+}/host	Pr^{4+}/trapped electron

[a] Note that A and A′ could not be discriminated.

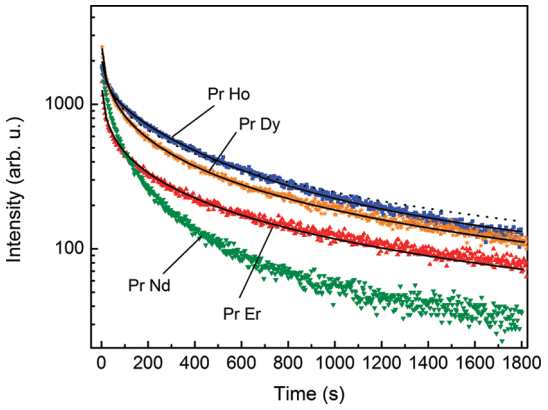

Figure 8. Persistent luminescence at T_{PL} = 293 K measured at 612 nm of the $YPO_4:Pr^{3+},Ln^{3+}$ compounds after 10 min of X-ray irradiation.

It appears that, in a wide range of trap depths, the product $\{T_m \exp(-E/kT_m)\}$ is constant within a few percent. Thus, for a given s and β, the trap depth E is quite accurately proportional to T_m. By fitting with a linear function the E values (obtained by the method of the shape of the glow curve) with the T_m temperatures, we thus obtained indicative E values for peaks A′, C, and C′ from their T_m value (see Table 2).

C. Long-Lasting Luminescence. Decays of long-lasting luminescence at 293 K over 30 min of (Pr^{3+},Ln^{3+})-codoped YPO_4 at 612 nm corresponding to the lifetime decay of the $^1D_2$ state of the Pr^{3+} ion are displayed in Figure 8. The most intense persistent luminescence is obtained for $YPO_4:Pr^{3+},Ho^{3+}$, followed by $YPO_4:Pr^{3+},Dy^{3+}$.

In the previous paragraph, we assumed that all the X_{Ln} and X'_{Ln} peaks were related to a first-order kinetics process where electrons get detrapped from Ln^{3+} codopants. We calculated activation energies E for each codopant (cf. Table 1). According to the well-known theory of thermoluminescence by Randall and Wilkins,[43] the decay of the long-lasting luminescence relative to such peaks can be expressed as

$$I(t) = I_0 \cdot \exp(-t/\tau) \text{ with } \tau = s^{-1} \cdot \exp(E/kT) \qquad (3)$$

where $I(t)$ is the intensity of luminescence, I_0 a constant, T the absolute temperature, E the activation energy, and s the frequency factor. In this way, the time constant τ represents the lifetime of the trapped charge at Ln^{3+}.

By taking into account only X'_{Ln} peaks, the decays of all $YPO_4:Pr^{3+},Ln^{3+}$ should, therefore, be purely monoexponential. Considering the temperature of the persistent luminescence experiment T_{PL} (293 K) and the position of each X'_{Ln} peak, only $YPO_4:Pr^{3+},Ho^{3+}$ should lead to measurable persistent luminescence over seconds/minutes because T_{PL} lies in the rise of its X'_{Ho} peak, as shown in Figure 5.[40] A very different pattern is actually observed in Figure 8. None of the decay is monoexponential, and all compounds show some long-lasting luminescence.

At this point, we should remember that the TSL experiments unravelled athermal tunneling processes in all the samples. In the TSL experiments, by the time the sample temperature reaches X'_{Ln}, that is, typically 20−35 min after the end of the irradiation, luminescence originating from athermal tunneling recombination is a background relative to the X'_{Ln} peak. However, immediately after the end of the irradiation, that is, at around 30 K in the TSL experiments, luminescence from tunneling recombination presents a very high intensity. Hence, in the persistent luminescence measurement at T_{PL}, luminescence emitted from athermal tunneling recombination may have a large influence on decays recorded over 30 min.

Tunneling recombination is known to depend both on the energetic height of the tunnel barrier and on the distance between the separated charges denoted as r. Tunneling for a

dx.doi.org/10.1021/jp108038v |J. Phys. Chem. C 2011, 115, 4217–4227

Table 3. Fitting Parameters for the Persistent Luminescence Decay Curves of Figure [8]

codopant	C_1	θ_0 (s)	C_2	τ (s)	R^2
Er	152 771	666			0.99195
Ho 1	340 714	856			0.98476
Ho 2	297 304	1098	370	357	0.99775
Dy	226 917	478			0.99854

given separation r results in monoexponential kinetics. However, irradiation creates a continuous distribution $n(r)$ of pairs of separated charges that finally results in a hyperbolic decay law:

$$I(t) = C/(1 + \lambda t) \quad (4)$$

In the present case, a simple hyperbolic law is not enough to be considered. An important parameter of our persistent luminescence measurement is the long-lasting irradiation time. Irradiation was indeed provided through a 10 min X-ray excitation process. In that case, some traps filled at a certain time within the irradiation time are detrapped before the irradiation is stopped. Within a short time, $d\theta$, during irradiation, some traps get filled and result in an afterglow $dI(t)$ showing the tunneling hyperbolic dependence

$$dI(t) = C_1\, d\theta/(t + \theta) \quad (5)$$

where C_1 is a constant corresponding to the irradiation and tunneling processes.[39] By summing up eq 5 over the whole irradiation time, θ_0, the intensity of tunneling afterglow follows the corrected hyperbolic law:[44,45]

$$I_{\theta 0}(t) = C_1/\theta_0 \ln(1 + \theta_0/t) \quad (6)$$

Let us start with $YPO_4:Pr^{3+},Er^{3+}$. We could observe on its glow curve in Figure 5 that the temperature at which persistent luminescence measurement is carried out (T_{PL} = 293 K) lies above the X'_{Er} peak. Hence, at T_{PL}, the recombination of charges separated as a hole on Pr^{3+} and an electron at Er^{3+} occurs quasi-immediately after the end of the excitation and no radiative recombination from these charges should be observed in the decay of Figure 8. Above, we have shown that trapped charges recombining by thermal assistance at peak D were already recombining by the tunnel effect at temperatures lower than peak D and higher than peak X'_{Er}. Hence, we suggest that the decay curve of $YPO_4:Pr^{3+},Er^{3+}$ originates from athermal tunneling recombination of trapped charges associated with peak D. To verify this assumption, the experimental decay of Figure 8 was fitted according to eq 6. The fitting curve is represented in Figure 8 as a continuous line, and the fitting parameters are presented in Table 3. A very good agreement was found as R^2 equals 0.99195. A value of 666 s was found for the parameter θ_0. This value is in total agreement with the actual irradiation time of 10 ± 2 min.

On the glow curve of $YPO_4:Pr^{3+},Dy^{3+}$ in Figure 5, T_{PL} lies at lower temperature than both X'_{Dy} and D peaks. Hence, no thermally activated recombination of holes at Pr^{3+} and electrons at Dy^{3+} and of charges associated with peak D should be at stake. Only tunneling between the opposite charges of these two couples may take place. Again, the experimental decay was fitted with eq 6 and an excellent agreement was found (R^2 = 0.99854). A value of 478 s was found for θ_0. This value is in line with the actual irradiation time of 10 ± 2 min.

The decay curve of $YPO_4:Pr^{3+},Ho^{3+}$ was first fitted in the same way by eq 6, which governs athermal tunneling. The fitting curve is displayed as a dotted line in Figure 8, and the fitting parameters are reported in Table 3 as Ho 1. For this compound, the agreement was found lower than for $YPO_4:Pr^{3+},Er^{3+}$ and $YPO_4:Pr^{3+},Dy^{3+}$ with R^2 = 0.98476. As T_{PL} lies in the rise of peak X'_{Ho} on the glow curve of Figure 5, the thermally activated peak should be taken into consideration. Hence, a fit of the decay by a sum of athermal tunneling and thermally assisted first-order kinetics was carried out, according to

$$I(t) = C_1/\theta_0 \cdot \ln(1 + \theta_0/t) + C_2 \cdot \exp(-t/\tau) \quad (7)$$

where C_2 is a constant corresponding to the thermally assisted process.

The resulting fitting line is shown in Figure 8 as a solid line, and the fitting parameters are shown in Table 3 as Ho 2. The agreement is good (R^2 = 0.99775).

Finally, the decay curve of $YPO_4:Pr^{3+},Nd^{3+}$ was found very difficult to be fitted. No simple tunneling or combination of tunneling and first-order thermally assisted process was found to well model the experimental decay. We relate this with a complicated pattern already observed in the TSL glow curve. We showed above that a high intensity of TSL background was present up to the X'_{Nd} peak, as a possible superimposition of several thermally assisted processes and tunneling. As T_{PL} lies just above the maximum of the X'_{Nd} peak, thermally assisted recombination of holes at Pr^{3+} and electrons at Nd^{3+} should occur very quickly before the first point of the curve is recorded. Nevertheless, other processes hidden in the background of the TSL glow curve at 293 K are most probably responsible for the complicated decay shown in Figure 8.

IV. DISCUSSION

A. Energetic Characterization and Identification of the Traps. YPO_4 is a model compound in spectroscopy as there is only one crystallographic site for Y^{3+} that can be easily substituted by any Ln^{3+}. Several studies, therefore, attempted to locate the energy levels of Ln^{3+} in yttrium phosphate. In Figure 9, we have reported as continuous lines the energy level diagram of the most recently published work on the topic.[28]

As demonstrated by Bos et al.[22] in Ce^{3+}-doped YPO_4, Ce^{3+} is a stable hole trap and acts as the recombination center, whereas Ln^{3+} (Ln = Dy^{3+}, Er^{3+}, Ho^{3+}, Nd^{3+}) codopants play the role of the electron traps (see Figure 9). The case of $YPO_4:Ce^{3+},Dy^{3+}$ is peculiar as the TSL of the compound at 370 K (peak X_{Dy}) shows in addition to the 5d−4f emission of Ce^{3+} the 4f−4f emission of Dy^{3+}. We could suppose that Dy^{3+} acts not only as an electron trap but also as an efficient recombination center and hole trap. However, the Dy^{3+} ground state is predicted at E_1 = 0.81 ± 0.5 eV above the top of the valence band and the activation energy for electron detrapping at Dy^{2+} was found at E_2 = 0.98 ± 0.04 eV, that is, at an energy too high for the hole to be still trapped at Dy^{3+}. We, therefore, propose the following explanation: in the recombination of the electron and hole at cerium, the released energy is not only used to excite cerium but also for close pairs of Ce^{3+},Dy^{3+}, the left behind dysprosium ion.

In the present work on $YPO_4:Pr^{3+},Ln^{3+}$, peaks denoted as X'_{Ln} were found to match very exactly to the corresponding X_{Ln} peaks in $YPO_4:Ce^{3+},Ln^{3+}$ for Ln = Er, Nd, Ho, and Dy. We found similar values of activation energies for electron detrapping from Ln^{2+} for both Pr^{3+}-doped and Ce^{3+}-doped YPO_4. From this, we drew the conclusion that Pr^{3+} is able to play a similar role to Ce^{3+}, that is, traps a hole and be a stable recombination center versus Er^{3+}, Nd^{3+}, Ho^{3+}, and Dy^{3+}. This is consistent with the predicted position of the Pr^{3+} ground state at 2.06 eV above the

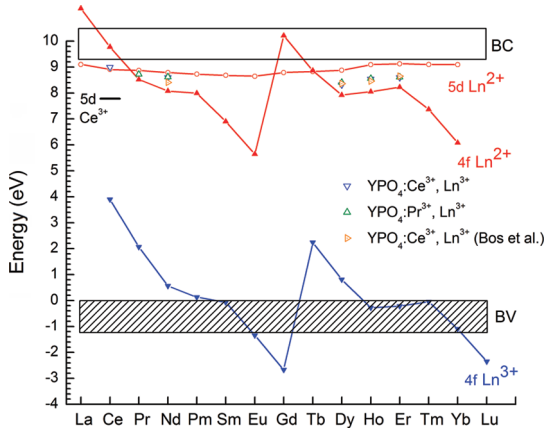

Figure 9. Energy level diagram of $YPO_4:Ln^{2+}$ and $YPO_4:Ln^{3+}$. Continuous lines for 4f Ln^{3+}, 4f Ln^{2+}, and 5d Ln^{2+} are taken from ref 28. The energy levels of Ln^{2+} based on the TSL activation energies derived from the peak shape method are displayed as empty points.

valence band in Figure 9. Each of the Ln^{3+} codopants selected here is then able to trap an electron in $YPO_4:Pr^{3+},Ln^{3+}$ in the same way as in $YPO_4:Ce^{3+},Ln^{3+}$. The determination of the trap depths of Ln^{2+} in $YPO_4:Pr^{3+},Ln^{3+}$ appears as an extra experimental evidence of the location of the ground state of the divalent lanthanide ions relative to the bottom of the conduction band (see Figure 9). Note that it is quite satisfying because consistent results were obtained with two different TSL set-ups: in the work of Bos et al., the TSL was run from room to high temperature with a fast heating rate (5 K/s) and operated on yttrium phosphate powders initially irradiated with γ-rays or β particles, whereas in the present work, the TSL was carried out from 30 K to high temperature applying a slow heating rate (10 K/min) and operated on a powder pellet irradiated with X-rays. Thus, the mechanism is not affected by the nature of the irradiation nor by the temperature at which the irradiation occurs. Similar to $YPO_4:Ce^{3+},Dy^{3+}$, in $YPO_4:Pr^{3+},Dy^{3+}$, the TSL was emitted via 4f−4f luminescence of Pr^{3+} as well as via 4f−4f luminescence of Dy^{3+}.

When we compared the activation energies with the Ln^{2+} ground states predicted by the energy level scheme, we noted a small systematic difference. The predicted trap depths (activation energies) are systematically 0.3−0.4 eV more shallow than the Ln^{2+} ground states. Such a difference is probably due to the two different experimental approaches. The TSL experiment probes the Ln^{2+} relaxed state, whereas the predictive model is based on charge-transfer (CT) states producing Ln^{2+} in the unrelaxed lattice with a hole on the nearest ligand. Hence, as the predictive model is based on optical (i.e., vertical on a configuration coordinate diagram) transitions, whereas our TSL measurements probe phonon-assisted (nonvertical) transitions, we could indeed expect to find smaller values with TSL experiments. Nevertheless, the predicted trend of the series of lanthanide ions is in perfect agreement with $E_{Dy} > E_{Ho} > E_{Er}$.

With the extended temperature range of TSL studied here, several other peaks appeared in addition to peaks X_{Ln} and X'_{Ln}. Peak A (at 100 K) and peak A′ (at 120 K) were observed in the glow curves of all Ce-doped compounds and absent in all Pr-doped ones. They are, therefore, associated with very much certainty to cerium. A trap depth of 0.2 eV was calculated for peak A and of 0.27 eV for peak A′ (see Table 2). According to the predicting energy level scheme of Figure 9, the Ce^{2+} $4f^2$ ground state is located inside the conduction band and, therefore, Ce^{3+} cannot trap an electron according to the scheme: $Ce^{3+} + e \rightarrow 4f^2$ Ce^{2+}. However, the 5d levels of Ce^{2+} are located below the conduction band,[28] and hence, electrons could be trapped according to the alternative scheme: $Ce^{3+} + e \rightarrow 4f^1 5d^1$ Ce^{2+}. According to Dorenbos's predictions shown in Figure 9, the first excited 5d state of Ce^{2+} is located at 0.38 eV below the conduction band. This value is consistent with the 0.2 eV (peak A) or 0.27 eV (peak A′) found for the trap depth of the Ce-related trap. We, therefore, think that peak A or peak A′ originates from detrapping of the electron from Ce^{2+} (= $Ce^{3+} + e$) and recombination with the hole left on another Ce^{3+}. Hence, A or A′ peak could actually be named X'_{Ce}. It is unfortunately not possible to discriminate between A and A′ as these peaks are very close in temperature and behavior.

Peaks B and B′ at around 195 K were found present on all compounds whatever the dopants and are correlated with a trap depth of 0.40 eV. Those peaks are, therefore, associated with an intrinsic defect of YPO_4. They might be associated with the thermal disintegration of excitonic species and local recombination processes as it is well documented on materials, such as $CdWO_4$ and $PbWO_4$,[46,47] for instance. More experimental evidence would be required to identify these defects in YPO_4.

Peak E (at 252 K) and peak D (at 480 K) were only observed on glow curves of Pr^{3+}-doped compounds. We have associated peak E, related to a trap depth of 0.58 eV, with the detrapping of electrons trapped at Pr^{3+} ions and recombination with holes located at other Pr^{3+} ions. According to Figure 9, the fundamental level of Pr^{2+} (= $Pr^{3+} + e$) is located around 0.68 eV below the conduction band at an intermediate value between Ce^{2+} and Nd^{2+}. Pr^{3+} should, therefore, be able to trap electrons at low temperature. The predicted value of 0.68 eV for Pr^{2+} is in good agreement with the experimentally determined value of 0.58 eV for electron trapping at Pr^{3+}, the systematic difference being this time only 0.1 eV.

Peak D (at 480 K) corresponding to a trap depth at 1.1 eV is absent on the glow curves of all the Ce^{3+}-doped samples and is present for all the Pr^{3+}-doped compounds. This can be interpreted in the light of very recent results on $YPO_4:Tb^{3+},Ln^{3+}$ compounds: when codoped by relatively deep electron traps (Ln^{3+} = Sm^{3+} or Tm^{3+}), these compounds show a high-temperature TSL peak displaying Sm^{3+}/Tm^{3+} f−f emission at 530 K corresponding to an activation energy of 1.54 eV. This activation energy is attributed to hole detrapping at Tb^{4+} leading to formation of a V_k-center, which then recombines at Sm^{2+}/Tm^{2+} electron centers.[48] According to the energy level prediction, hole detrapping from Pr^{4+} should occur at a 0.2 eV smaller energy than from Tb^{4+}, that is, at around 1.3 eV. This value corresponds within the error bars to the 1.1 eV activation energy for peak D. However, in the case of our Pr-doped samples, no obvious emitting electron-trap center is available in the material and f−f Pr^{3+} emission is still observed. We, therefore, propose the hypothesis of a nonemitting unidentified deep electron trap center that would recombine with the mobile V_k-center and subsequently excite Pr^{3+}. Alternatively, it is worth noting that Vedda et al. observed quite similar TSL behavior for $Ce^{3+}/Tb^{3+}/Pr^{3+}$-doped $YAlO_3$ and suggested the existence of defect complexes involving intrinsic defects coupled to $Ce^{3+}/Pr^{3+}/Tb^{3+}$ ions in which carriers can be transferred from intrinsic levels to the rare earth ion levels where the radiative recombination occurs. We think that more experimental evidence is necessary to ascertain one or the other interpretation of our Pr-related 480 K TSL peak.

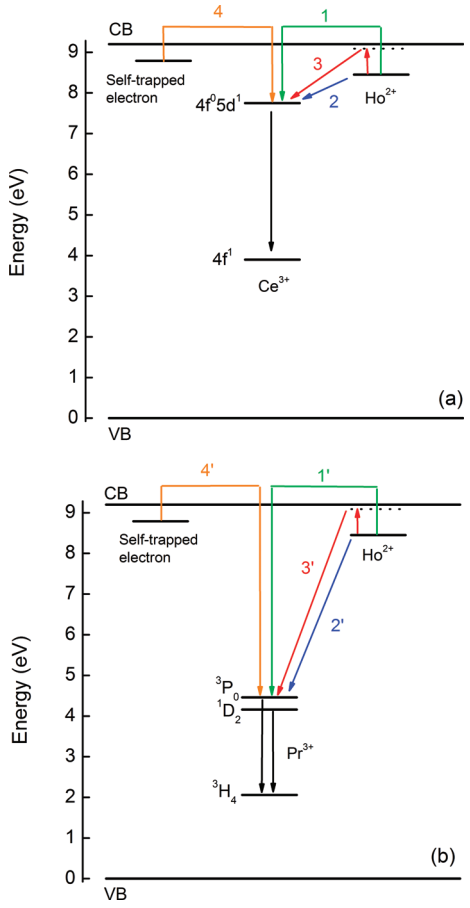

Figure 10. Energy scheme of trapping centers in (a) $YPO_4:Ce^{3+},Ho^{3+}$ and (b) $YPO_4:Pr^{3+},Ho^{3+}$ and mechanisms of recombination.

Peaks C and C′ at around 135 K were only observed on glow curves of Nd^{3+}-codoped compounds but could unfortunately not be explained here.

The various hypotheses proposed here are summarized in Table 2 (column 4) along with the trapping mechanism (column 5). The energy scheme of all the traps is displayed in Figure 10 and is commented below.

B. Mechanisms of Delayed Luminescence in YPO_4. Figure 10 presents the proposed mechanisms of recombination of trapped charges at stake in YPO_4 compounds. Note that Figure 10 presents an energy scheme for $Ln^{3+} = Ho^{3+}$ as an instance, but the whole discussion is valid for Ln = Ce, Pr, Nd, Dy, and Er instead of Ln = Ho. The thermally and conduction band-assisted processes first demonstrated in $YPO_4:Ce^{3+},Ln^{3+}$[22] are represented as process 1 (peaks X_{Ln}). They were shown here to happen as well in $YPO_4:Pr^{3+},Ln^{3+}$ (process 1′ in Figure 10 corresponding to peaks X'_{Ln}).

The TSL measurements here carried out from 30 K revealed an important part of athermal tunneling recombination. In the TSL glow curves of $YPO_4:Ce^{3+}$ and $YPO_4:Ce^{3+},Ln^{3+}$, tunneling luminescence was found to be suppressed after peak X_{Ln}. Therefore, tunneling is thought to happen in $YPO_4:Ce^{3+},Ln^{3+}$ between holes at Ce^{3+} sites and electrons at Ln^{3+} sites. In $YPO_4:Pr^{3+},Ln^{3+}$, some TSL intensity is similarly suppressed after the X'_{Ln} peak, implying tunneling between holes at Pr^{3+} and electrons at Ln^{3+}. These athermal tunneling recombination mechanisms are shown as processes 2 and 2′ in $YPO_4:Ce^{3+},Ho^{3+}$ and in $YPO_4:Pr^{3+},Ho^{3+}$, respectively, in the schemes of Figure 10. Athermal tunneling followed by Ce, respectively, Pr emission (i.e., radiative recombination) is possible because the emitting excited states of Ce^{3+} ($4f^15d^1$) and Pr^{3+} ($^3P_0$ and $^1D_2$) are at lower energy than the Ho^{2+} ground state.

The high background or prepeak luminescence ascribed to athermal tunneling seems not fully independent of the temperature. Indeed, in the TSL experiment, this background was not decreasing over time but was increasing with temperature over the range of 70−300 K in a degree depending of the dopant. We may suppose a distribution of shallow unidentified traps that would give rise to a multitude of overlapping peaks. However, it is striking to observe that this increasing TSL background is always suppressed after the corresponding TSL peak whatever its position ranging from 120 K in $YPO_4:Ce^{3+}$ to 370 K in $YPO_4:Ce^{3+},Dy^{3+}$. We would then rather propose an explanation similar to what was proposed by Nikl et al. in ref 49 for a similar increasing TSL intensity following tunneling decay in $Lu_3Al_5O_{12}$:Ce. The increasing TSL intensity may correspond to thermally assisted tunneling occurring between the same centers. In the case of X_{Ln} or X'_{Ln} peaks, thermal energy below the TSL peak would allow tunneling from an excited state of the electron center Ln^{2+} to the Pr^{4+}/Ce^{4+} recombination center, as shown by processes 3 and 3′ in Figure 10 Thermally assisted tunneling from excited d states of Sm^{2+} to Ce^{4+} was actually demonstrated in $YPO_4:Ce^{3+},Sm^{3+}$.[27,28]

Peaks B and B′ were demonstrated to be present in all samples and attributed to self-trapped charges. Recombination on Ce^{3+}/Pr^{3+} can occur through band-assisted thermal release of a self-trapped electron shown as processes 4/4′ or through a local thermally assisted tunneling process as in tungstates.[46,47]

C. A Method to Induce Long-Lasting Luminescence ? With the YPO_4 model compound, we have shown that some red long-lasting luminescence could be obtained by Pr^{3+} doping and Ln^{3+} codoping. Although we pointed out that the best Ln^{3+} codopant to induce persistent luminescence at room temperature by a thermally assisted mechanism would be Ho^{3+}, we showed that athermal tunneling processes are responsible for an important part of the decay. Note that the position of the TSL peak X'_{Ln} has an indirect influence on persistent luminescence: the temperature at which persistent luminescence is measured, T_{PL}, was situated at lower temperature than X'_{Ln} so that charges were still separated at $(Pr^{3+}-Ln^{3+})$ couples at T_{PL} and tunneling recombination could take place. This explains why both $YPO_4:Pr^{3+},Ho^{3+}$ and $YPO_4:Pr^{3+},Dy^{3+}$ showed better long-lasting luminescence than $YPO_4:Pr^{3+},Er^{3+}$ and $YPO_4:Pr^{3+},Nd^{3+}$. Considering that athermal tunneling plays an important role in the persistent luminescence decays, one may tune the intensity of persistent luminescence by varying the concentrations of dopant and codopant because tunneling is very much affected by the distance between separated charges.[39]

In YPO_4:0.5% Pr^{3+},0.5% Ln^{3+}, it appears difficult to obtain long-lasting luminescence governed by a thermally and band-assisted process because tunneling recombination is the dominant process. In the view of designing new persistent phosphors, this raises the question of whether tunneling is related to the $YPO_4:Ln^{3+}$ material or if this is a very general phenomenon present in most compounds and, therefore, difficult to avoid. Visocekas observed the tunneling effect in calcite $CaCO_3$[50,51] as well as in $CaSO_4$:Dy, $Li_2B_4O_7$:Cu, alumina, and $LaMgAl_{11}O_{19}$,[52] and in many feldspars.[53] Other studies report tunneling in ZnS:Cu,[54] KCI:TICI,[44] amorphous glass, zircon,[55] and Zn_2SiO_4:Mn.[56] There are many reports on materials showing anomalous

dx.doi.org/10.1021/jp108038v |J. Phys. Chem. C 2011, 115, 4217–4227

fading, which is a direct consequence of tunneling recombination.[41,56,57] Finally, Visocekas concludes that tunneling tends to happen when too many defects are present in the material, for instance, when impurities are present.[39] If one wants to design a new persistent phosphor by adding impurities to a material, it may, therefore, be very difficult to avoid tunneling recombination. On the other hand, if a controlled pure tunneling phenomenon could be induced in a material with a sufficient amount of trapped charges to produce intense long-lasting luminescence, this material would present a real advantage for applications, such as in vivo imaging: its persistent luminescence decay would not be temperature-dependent.

V. CONCLUSIONS

In this work, YPO_4 appeared one more time as a very good model compound to investigate the mechanisms of charge trapping and detrapping related to doping with lanthanides. By replacing in the present work Ce^{3+} by Pr^{3+} in the series of compounds YPO_4:Ce^{3+},Ln^{3+}, the predictions of Dorenbos as well as the previous attributions of TSL peaks to electron trapping at Ln^{3+} (Ln = Nd, Dy, Ho, Er) by Bos et al. were confirmed. Pr^{3+} was shown to play a similar role to Ce^{3+}, namely, as a hole trap and recombination center, in line with the predicted position of its ground state relative to the valence band. With TSL measurements realized here over an extended temperature range, two new attributions were proposed: detrapping of electrons from Ce^{3+} at 100 K (or 120 K) and from Pr^{3+} at 252 K. Values of trap depths of 0.2 eV (or 0.27 eV) and 0.58 eV were found consistent with the position of the ground state of, respectively, Ce^{2+} and Pr^{2+} from the bottom of the conduction band. Two other TSL peaks possessing a very systematic behavior along the series of YPO_4:Ce^{3+},Ln^{3+} and YPO_4:Pr^{3+},Ln^{3+} were observed. A peak at 480 K was surely associated with praseodymium and was tentatively explained by the hole release from Pr^{4+}. A peak at 195 K corresponding to a trap depth of 0.41 eV was consistently observed in all the 10 studied compounds and presumably associated with a self-trapped electron in the host. However, one would need complementary experimental evidence to verify these last assumptions. Techniques, such as electron paramagnetic resonance, should be used to physically identify the defects.

From the position of the TSL peaks around room temperature and their first-order kinetics reported by Bos et al. for YPO_4:Ce^{3+},Ln^{3+} (Ln = Nd, Dy, Ho, Er), we were expecting thermally and band-assisted persistent luminescence at room temperature. We showed that replacing the recombination center Ce^{3+} by Pr^{3+} was a right option to obtain orange/red luminescence instead of blue as Pr^{3+} was very much behaving like Ce^{3+}. Nevertheless, the shape of the measured persistent luminescence decays of YPO_4:Pr^{3+},Ln^{3+} were found very different from expected. We showed that an important phenomenon of radiative recombination by tunneling was taking part in detrapping at Ln^{3+} species. The persistent luminescence decays at room temperature were very well fitted by a tunneling phenomenon, mainly athermal, and that could be as well observed at 30 K in the beginning of the TSL curves. The analysis of the TSL curves showed that two distinct couples of separated charges were implied in the radiative recombination by tunneling: on the one hand, the same couple as in the $(Pr^{3+},Ln^{3+}) \rightarrow (Pr^{4+},Ln^{2+})$ process, and on the other hand, the same couple as the one implied in the 480 K TSL peak present on all Pr-doped compounds.

With this paper, we presented a way to design a red long-lasting luminescence material from the knowledge of lanthanide dopants' energy levels. We showed that the mechanism of detrapping and recombination is also very important to consider as tunneling was here governing very largely persistent luminescence decays. Such a study can help us to design new persistent phosphors as well as, in a more general manner, new charge storage materials.

AUTHOR INFORMATION

Corresponding Author

*Telephone: 33 (0)1 53 73 79 43. Fax: 33 (0)1 46 34 74 89. E-mail: aurelie-bessiere@chimie-paristech.fr.

ACKNOWLEDGMENT

This work was supported by the Medicen project of Ile-de-France and the Natlurim ANR project. The authors would like to thank Pr. D. Gourier for fruitful discussions.

REFERENCES

(1) Matsuzawa, T.; Aoki, Y.; Takeuchi, N.; Murayama, Y. *J. Electrochem. Soc.* **1996**, *143*, 2670–2673.
(2) Jia, D.; Jia, W.; Evans, D. R.; Dennis, W. M.; Liu, H.; Zhu, J.; Yen, W. M. *J. Appl. Phys.* **2000**, *88*, 3402–3407.
(3) Pan, Y.; Su, Q.; Chen, T.; Ge, W.; Yang, C.; Wu, M. *J. Solid State Chem.* **2003**, *174*, 69–73.
(4) Wang, X. J.; Jia, D.; Yen, W. M. *J. Lumin.* **2003**, *102*−103, 34–37.
(5) Yu, X. B.; Mao, L. H.; Fan, Z.; Yang, L. Z.; Yang, S. P. *Mater. Lett.* **2004**, *58*, 3661–3664.
(6) Wang, X.; Zhang, Z.; Tang, Z.; Lin, Y. *Mater. Chem. Phys* . **2003**, *80*, 1–5.
(7) Van Den Eeckhout, K.; Smet, P. F. *J. Lumin.* **2009**, *129*, 1140–1143.
(8) Smet, P. F.; Avci, N.; Poelman, D. *J. Electrochem. Soc.* **2009**, *156*, H243–H248.
(9) Le Masne de Chermont, Q.; Chanéac, C.; Seguin, J.; Pellé, F.; Maîtrejean, S.; Jolivet, J.-P.; Gourier, D.; Bessodes, M.; Scherman, D. *Proc. Natl. Acad. Sci.* **2007**, *104*, 9266–9271.
(10) Le Masne de Chermont, Q.; Scherman, D.; Bessodes, M.; Pellé, F.; Maîtrejean, S.; Jolivet, J.-P.; Chanéac, C.; Gourier, D. Patent WOEP06067950, WO2007048856, 30/10/2006.
(11) Lecointre, A.; Viana, B.; LeMasne, Q.; Bessière, A.; Chanéac, C.; Gourier, D. *J. Lumin.* **2009**, *129*, 1527–1530.
(12) Lecointre, A.; Bessière, A.; Viana, B.; Gourier, D. *Radiat. Meas.* **2010**, *45*, 497–499.
(13) Lecointre, A.; Bessière, A.; Viana, B.; Aït Benhamou, R.; Gourier, D. *Radiat. Meas.* **2010**, *45*, 273–276.
(14) Rambabu, U.; Munirathnam, N. R.; Prakash, T. L.; Buddhudu, S. *Mater. Chem. Phys.* **2003**, *78*, 160–169.
(15) Begun, G. M.; Beall, G. W.; Boatner, L. A.; Gregor, W. J. *J. Raman Spectrosc.* **1981**, *11*, 273–278.
(16) Hayhurst, T.; Shalimoff, G.; Conway, J. G.; Edelstein, N.; Boatner, L. A.; Abraham, M. M. *J. Chem. Phys.* **1982**, *76*, 3960–3966.
(17) Nakazawa, E.; Shiga, F. *J. Lumin.* **1977**, *15*, 255–259.
(18) Blasse, G.; Grabmaier, B. C. *Luminescent Materials*; Springer: Berlin, 1994.
(19) Nirwan, F. M.; Gundu Rao, T. K.; Gupta, P. K.; Pode, R. B. *Phys. Status Solidi A* **2003**, *198*, 447.
(20) Jung, K. Y.; Lee, K. K.; Kang, Y. C.; Park, H. D. *J. Mater. Sci. Lett.* **2003**, *22*, 1527–1529.
(21) Wu, C.; Wang, Y.; Jie, W. *J. Alloys Compd.* **2007**, *436*, 383–386.
(22) Bos, A. J. J.; Dorenbos, P.; Bessière, A.; Viana, B. *Radiat. Meas.* **2008**, *43*, 222–226.
(23) Dorenbos, P. *J. Phys.: Condens. Matter* **2003**, *15*, 8417–8434.

(24) Dorenbos, P. *J. Lumin.* **2005**, *111*, 89–104.
(25) Dorenbos, P. *Opt. Mater.* **2009**, *488*, 568–573.
(26) Krumpel, A. H.; Bos, A. J. J.; Bessière, A.; Van Der Kolk, E.; Dorenbos, P. *Phys. Rev. B* **2009**, *80*, 085103.
(27) Bos, A. J. J.; Poolton, N. R. J.; Wallinga, J.; Bessière, A.; Dorenbos, P. *Radiat. Meas.* **2010**, *45*, 343–346.
(28) Poolton, N. R. J.; Bos, A. J. J.; Jones, G. O.; Dorenbos, P. *J. Phys.: Condens. Matter* **2010**, *22*, 185403.
(29) Dorenbos, P.; Bos, A. J. J. *Radiat. Meas.* **2008**, *43*, 139–145.
(30) Di, W.; Wang, X.; Chen, B.; Lai, H.; Zhao, X. *Opt. Mater.* **2005**, *27*, 1386–1390.
(31) Moune, O. K.; Faucher, M. D.; Edelstein, N. *J. Lumin.* **2002**, *96*, 51–68.
(32) De Mello Donega, C.; Meijerink, A.; Blasse, G. *J. Phys. Chem. Solids* **1995**, *56*, 673–685.
(33) Chen, H.; Lian, R.; Yin, M.; Lou, L.; Zhang, W.; Xia, S.; Krupa, J.-C. *J. Phys.: Condens. Matter* **2001**, *13*, 1151–1158.
(34) Pinel, E.; Boutinaud, P.; Mahiou, R. *J. Alloys Compd.* **2004**, *374*, 165–168.
(35) Van Pieterson, L.; Reid, M. F.; Wegh, R. T.; Soverna, S.; Meijerink, A. *Phys. Rev. B* **2002**, *65*, 045114.
(36) Karanjikar, N. P.; Naik, R. C. *Solid State Commun.* **1988**, *65*, 1419–1422.
(37) Lai, H.; Bao, A.; Yang, Y.; Xu, W.; Tao, Y.; Yang, H. *J. Lumin.* **2008**, *128*, 521–524.
(38) Vedda, A.; Fasoli, M.; Nikl, M.; Laguta, V. V.; Mihokova, E.; Pejchal, J.; Yoshikawa, A.; Zhuravleva, M. *Phys. Rev. B.* **2009**, *80*, 045113.
(39) Visocekas, R. *Radiat. Prot. Dosim.* **2002**, *100*, 45–54.
(40) Visocekas, R. *La luminescence de la calcite après irradiation cathodique: Thermoluminescence et luminescence par effet tunnel*. Ph.D. Thesis, Université P et M Curie, 1979.
(41) McKeever, S. W. S. *Thermoluminescence of Solids*; Cambridge University Press: Cambridge, U.K., 1985.
(42) Chen, R. *J. Electrochem. Soc.* **1969**, *116*, 1254.
(43) Randall, J. T.; Wilkins, M. H. F. *Proc. R. Soc. A* **1945**, *184*, 366.
(44) Delbecq, C. J.; Toyozawa, Y.; Yuster, P. H. *Phys. Rev. B* **1974**, *9*, 4497–4505.
(45) Poolton, N. R. J.; Kars, R. H.; Wallinga, J.; Bos, A. J. J. *J. Phys.: Condens. Matter* **2009**, *21*, 485505.
(46) Martini, M.; Meinardi, F.; Spinolo, G.; Vedda, A.; Nikl, M.; Usuki, Y. *Phys. Rev. B* **1999**, *60*, 4653–4658.
(47) Fabeni, P.; Kiisk, V.; Krasnikov, A.; Nikl, M.; Pazzi, G. P.; Sildos, I.; Zazubovich, S. *Phys. Status Solidi C* **2007**, *4*, 918–921.
(48) Bos, A. J. J.; Dorenbos, P.; Bessière, A.; Lecointre, A.; Bedu, M.; Bettinelli, M.; Piccinelli, F. *Radiat. Meas.*, 2010, submitted for publication.
(49) Nikl, M.; Vedda, A.; Fasoli, M.; Fontana, I.; Laguta, V. V.; Mihokova, E.; Pejchal, J.; Rosa, J.; Nejezchleb, K. *Phys. Rev. B* **2007**, *76*, 195121.
(50) Visocekas, R.; Ceva, T.; Marti, C.; Lefaucheux, F.; Robert, M. C. *Phys. Status Solidi A* **1976**, *35*, 315–327.
(51) Visocekas, R.; Geoffroy, A. *Phys. Status Solidi A* **1977**, *41*, 499–503.
(52) Visocekas, R. *Nucl. Tracks Radiat. Meas.* **1988**, *14*, 163–168.
(53) Visocekas, R.; Spooner, N. A.; Zink, A.; Blanc, P. *Radiat. Meas.* **1994**, *23*, 377–385.
(54) Riehl, N. *J. Lumin.* **1970**, *1*−2, 1–16.
(55) Templer, R. H. *Nucl. Tracks Radiat. Meas.* **1985**, *10*, 531–537.
(56) Avouris, P.; Morgan, T. N. A. *J. Chem. Phys.* **1981**, *74*, 4347–4355.
(57) Chen, R.; Kirsh, Y. *Analysis of Thermally Stimulated Processes*; International Series on the Science of the Solid State; Pergamon Press: Oxford, U.K., 1981.